Electrochimica Acta 58 (2011) 406–416

Contents lists available at SciVerse ScienceDirect

Electrochimica Acta

journal homepage: www.elsevier.com/locate/electacta

Generalized study of the temporal behaviour in recirculating electrochemical reactor systems

A.N. Colli, J.M. Bisang*

Programa de Electroquímica Aplicada e Ingeniería Electroquímica (PRELINE), Facultad de Ingeniería Química, Universidad Nacional del Litoral, Santiago del Estero 2829, S3000AOM Santa Fe, Argentina

ARTICLE INFO

Article history:
Received 28 June 2011
Received in revised form
19 September 2011
Accepted 22 September 2011
Available online 1 October 2011

Keywords:
Flow reactors
Mass-transfer coefficient
Non-ideal behaviour
Rotating cylinder electrode

ABSTRACT

This paper outlines and compares mathematical models to predict the temporal variation of concentration and current in an electrochemical reactor coupled with a reservoir operating with continuous recirculation of the electrolyte. The reservoir is considered as a well mixed tank while the dispersion model is used for the reactor. The performances according to the idealized models to represent a reactor, stirred tank and plug flow, are also deduced as limiting cases. Applied studies carried out in rotating cylinder electrodes using the removal of copper from dilute solutions as test reaction are reported. The experimental data are correlated with the theoretical model, numerically solved, using a dimensionless number β, proportional to the kinetic constant, as fitting parameter. The results in accordance with this rigorous model are compared with those of the conventional equations based on the stirred tank model and the error in the evaluation of the kinetic constant can be as high as 26%. From an engineering point of view, a generalized plot to estimate the error is reported, which requires as inputs the experimental slope of the temporal variation of concentration in the reservoir, the Peclet number and the ratio between the reservoir and reactor space times.

1. Introduction

The use of an electrochemical reactor coupled with a reservoir is a common arrangement in industrial practice. The reservoir allows extraction of products or input of reactants, heat exchange, additive addition, control operations and the treatment of a large volume of effluent in a small reactor. Several authors have treated the mathematical modelling of this electrochemical system. Pickett [1] analyzed a batch electrochemical reactor with continuously recirculating electrolyte in which a mass-transfer controlled reaction and perfect mixing in the reactor were assumed. Walker and Wragg [2] developed approximate and rigorous models considering the reservoir as a well-mixed tank while the reactor was considered both as a plug flow and as a perfectly back-mixed item. Mustoe and Wragg [3] took into account axial dispersion in the reactor in the prediction of the temporal behaviour for a large reservoir to reactor volume ratio. Schaller and Kreysa [4] presented a rigorous treatment assuming plug flow in the reactor with a constant inlet concentration and Thomas and Sora [5] reported an alternative expression to that proposed in [2] for a plug flow reactor coupled with a well-mixed reservoir.

Recently the arrangement of continuous recirculation from a large storage tank to a small electrochemical reactor has received considerable attention in the processing of effluents. Thus, the reduction of Cr(VI) to Cr(III) was achieved in a flow-by parallel-plate reactor with recirculation, equipped with a reticulated vitreous carbon electrode [6]. A similar arrangement was used [7] to study the removal of copper under different hydrodynamic and kinetic conditions. Lanza and Bertazzoli [8] designed a reactor with a $Ti/70TiO_2/30RuO_2$ DSA-type anode for cyanide electrooxidation in batch recirculating mode. The device performance was evaluated in terms of the decay of the cyanide concentration as a function of the current density, flow rate and initial pollutant concentration.

The main objective of this work is to present a rigorous model for a recirculating electrochemical system assuming the dispersion model for the reactor. The rigorous model is compared to the conventional equations for this system to determine their validity ranges. The theoretical data are compared with experimental results using copper deposition as test reaction in an electrochemical reactor with rotating cylinder electrodes.

* Corresponding author.
E-mail address: jbisang@fiq.unl.edu.ar (J.M. Bisang).

0013-4686/$ – see front matter © 2011 Elsevier Ltd. All rights reserved.
doi:10.1016/j.electacta.2011.09.058

2. Models for a recirculating electrochemical reactor system

2.1. Concentration as a function of time

2.1.1. Dispersion model, DM

The temporal behaviour of an electrochemical reactor according to the dispersion model is given by

$$\tau_R \frac{\partial c(t,\ y)}{\partial t} = \frac{1}{\mathrm{Pe}} \frac{\partial^2 c(t,\ y)}{\partial y^2} - \frac{\partial c(t,\ y)}{\partial y} - \frac{j(t,\ y)\, a_e \tau_R}{\nu_e F \varepsilon} \quad (1)$$

where

$$\tau_R = \frac{\varepsilon L}{u} \quad (2)$$

$$\mathrm{Pe} = \frac{uL}{\varepsilon D_L} \quad (3)$$

$$\text{and} \quad y = \frac{x}{L} \quad (4)$$

c (mol m^{-3}) being the concentration, Pe the Peclet number, t (s) the time, τ_R (s) the reactor space time, L (m) the electrode length, u (m s^{-1}) the mean superficial fluid velocity, ε the porosity, D_L (m^2 s^{-1}) the dispersion coefficient, x (m) the axial coordinate and y the normalized axial coordinate.

Under potentiostatic operation the kinetics of a first order reaction at high electrode potentials is given by [9]

$$j(t, y) = \nu_e F k c(t, y) \quad (5)$$

here j (A m^{-2}) is the current density, ν_e is the number of electrons interchanged, F (96,485 C mol^{-1}) is the Faraday constant and k (m s^{-1}) is a kinetic constant given by:

$$k = \frac{k_f}{1 + \mathrm{Da}} \quad (6)$$

k_f (m s^{-1}) being the rate constant and Da the Damköhler number defined as k_f/k_m, where k_m (m s^{-1}) is the mass-transfer coefficient.

Usually the reactor volume is lower than the reservoir volume. Then, the temporal behaviour of the system is determined by the reservoir volume. Thus, it is convenient to define a dimensionless time, T, as

$$T = \frac{t}{\tau_M} \quad (7)$$

here τ_M (s) is the reservoir space time. Introducing Eqs. (5)–(7) into Eq. (1) and rearranging results in

$$\frac{1}{R} \frac{\partial C(T, y)}{\partial T} = \frac{1}{\mathrm{Pe}} \frac{\partial^2 C(T, y)}{\partial y^2} - \frac{\partial C(T, y)}{\partial y} - \beta C(T, y) \quad (8)$$

with the following initial and boundary conditions, valid for a closed system at the inlet, Eq. (10), and at the outlet, Eq. (11)

$$T = 0 \quad C(0, y) = 1 \quad (9)$$

$$y = 0 \quad \text{and} \quad T > 0 \quad C(T, 0) - \frac{1}{\mathrm{Pe}} \left.\frac{\partial C(T, y)}{\partial y}\right|_{y=0} = C_i(T) \quad (10)$$

$$y = 1 \quad \left.\frac{\partial C(T, y)}{\partial y}\right|_{y=1} = 0 \quad (11)$$

where

$$C(T, y) = \frac{c(T, y)}{c^0} \quad (12)$$

here c^0 (mol m^{-3}) is the initial concentration,

$$R = \frac{\tau_M}{\tau_R} \quad (13)$$

$$\text{and} \quad \beta = \frac{k a_e \tau_R}{\varepsilon} \quad (14)$$

Thus, β is a useful dimensionless number which lumps the electrochemical kinetics, k, geometrical aspects of the electrode such as the specific surface area, a_e (m^{-1}), and ε, with the reactor space time.

The mass-balance in the reservoir gives

$$\frac{dC_i(T)}{dT} = C_o(T) - C_i(T) \quad (15)$$

where the subscripts "i" and "o" denote the dimensionless concentration at the inlet and at the outlet of the reactor, respectively.

Applying Laplace transformation to Eq. (8) yields

$$\bar{C}_o(s) = (s + \beta R)^{-1} + 4\sigma e^{\mathrm{Pe}/2} \frac{\bar{C}_i(s) - (s + \beta R)^{-1}}{(\sigma + 1)^2 e^{\sigma \mathrm{Pe}/2} - (\sigma - 1)^2 e^{-\sigma \mathrm{Pe}/2}} \quad (16)$$

where

$$\sigma = \sqrt{1 + 4(\beta R + s)(R\mathrm{Pe})^{-1}} \quad (17)$$

Applying Laplace transformation to Eq. (15) and combining with Eq. (16) results in

$$\bar{C}_i(s) = \frac{1 + (s + \beta R)^{-1}[1 - 4\sigma e^{\mathrm{Pe}/2}/((\sigma + 1)^2 e^{\sigma \mathrm{Pe}/2} - (\sigma - 1)^2 e^{-\sigma \mathrm{Pe}/2})]}{s + 1 - 4\sigma e^{\mathrm{Pe}/2}/((\sigma + 1)^2 e^{\sigma \mathrm{Pe}/2} - (\sigma - 1)^2 e^{-\sigma \mathrm{Pe}/2})} \quad (18)$$

The inversion of Eq. (18) from the complex s plane to the T time plane was made by a numerical Laplace transform inversion method [10], using a Fourier series approximation with a Matlab subroutine [11].

2.1.2. Dispersion model at high R values

For $R \gg 1$ Eq. (8) is simplified to

$$\frac{1}{\mathrm{Pe}} \frac{d^2 C(y)}{dy^2} - \frac{dC(y)}{dy} - \beta C(y) = 0 \quad (19)$$

Solving Eq. (19) taking into account the boundary conditions of Eqs. (10) and (11), yields [12]

$$C(T, y) = 2 \frac{(\alpha + 1) e^{(1-y)\alpha \mathrm{Pe}/2} + (\alpha - 1) e^{-(1-y)\alpha \mathrm{Pe}/2}}{(\alpha + 1)^2 e^{\alpha \mathrm{Pe}/2} - (\alpha - 1)^2 e^{-\alpha \mathrm{Pe}/2}} e^{y \mathrm{Pe}/2} C_i(T) \quad (20)$$

$$\text{where} \quad \alpha = \sqrt{1 + \frac{4\beta}{\mathrm{Pe}}} \quad (21)$$

Evaluating Eq. (20) at $y = 1$ and combining with Eq. (15) gives

$$\frac{dC_i(T)}{dT} = -C_i(T) \left[1 - \frac{4\alpha e^{\mathrm{Pe}/2}}{(\alpha + 1)^2 e^{\alpha \mathrm{Pe}/2} - (\alpha - 1)^2 e^{-\alpha \mathrm{Pe}/2}}\right] \quad (22)$$

Integrating Eq. (22) with the initial condition, Eq. (9), results in

$$C_i(T)\big|_{\mathrm{DM}, R \to \infty} = \exp\left\{-\left[1 - \frac{4\alpha e^{\mathrm{Pe}/2}}{(\alpha + 1)^2 e^{\alpha \mathrm{Pe}/2} - (\alpha - 1)^2 e^{-\alpha \mathrm{Pe}/2}}\right] T\right\} \quad (23)$$

Eq. (23) was previously reported by Mustoe and Wragg [3].

2.1.3. Stirred tank model (Pe → 0), ST

The mass-balance for the reactor yields

$$\frac{1}{R} \frac{dC_o(T)}{dT} = C_i(T) - (1 + \beta) C_o(T) \quad (24)$$

Combining Eqs. (15) and (24), results in

$$\frac{d^2 C_i(T)}{dT^2} + [1 + R(1 + \beta)] \frac{dC_i(T)}{dT} + R\beta C_i(T) = 0 \quad (25)$$

With the following initial conditions

$$T = 0 \quad C_i(0) = 1 \quad (26)$$

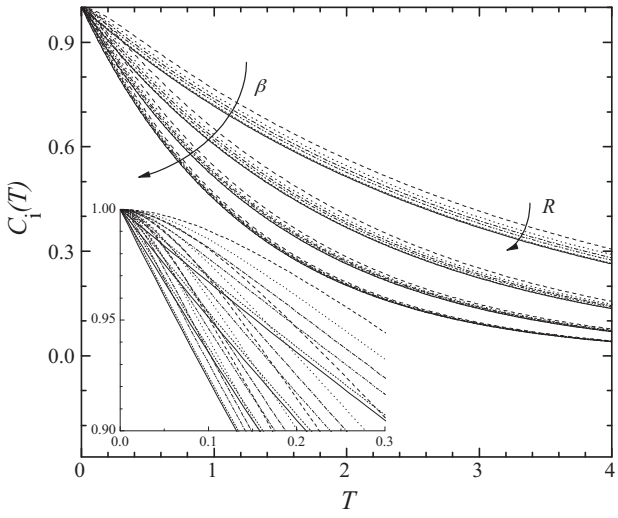

Fig. 1. Dimensionless concentration in the reservoir as a function of time for a stirred tank electrochemical reactor coupled with a reservoir according to Eq. (28) for different values of β and R. β values: 0.5, 1, 2, and 4. R values: 5, 8, 12, 20, and 100. Full lines: behaviour according to Eq. (30). Inset: exploded view at low T values.

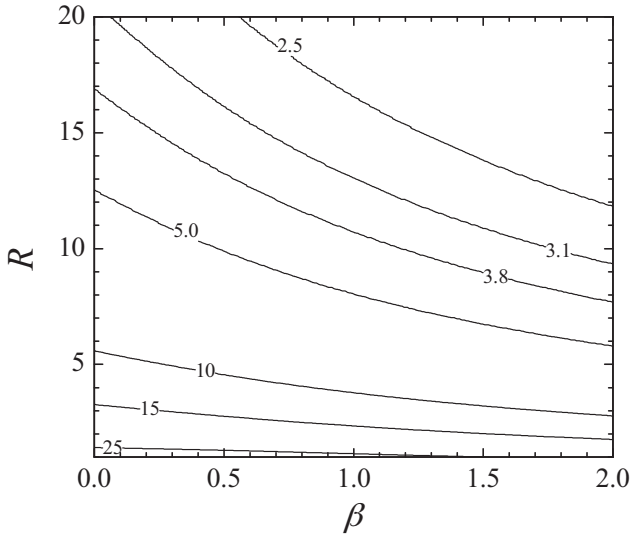

Fig. 2. Contour plots of λ, Eq. (31), for a stirred tank electrochemical reactor coupled with a reservoir as a function of β and R. Contour height numbers are λ values.

and from Eq. (15)

$$\left.\frac{dC_i(T)}{dT}\right|_{T=0} = 0 \tag{27}$$

Solving Eq. (25) yields

$$C_i(T)|_{ST} = \frac{1}{r_2 - r_1}(r_2 e^{r_1 T} - r_1 e^{r_2 T}) \tag{28}$$

where

$$r_{1,2} = -\frac{1 + R(1+\beta)}{2} \pm \frac{\sqrt{[1+R(1+\beta)]^2 - 4\beta R}}{2} \tag{29}$$

Pickett [1] proposed a similar equation valid when the mixer volume is negligible.

2.1.4. Stirred tank model at high R values

When the Pe number approaches zero, Eq. (23) yields

$$C_i(T)|_{ST,R\to\infty} = e^{-[\beta/(1+\beta)]T} \tag{30}$$

Fig. 1 shows the dimensionless concentration in the reservoir as a function of the dimensionless time at different values of β and R for the model of a stirred tank electrochemical reactor coupled with a reservoir, Eq. (28). The inset corresponds to the behaviour at the beginning of the experiment. The behaviour according to Eq. (30), assuming that the reservoir volume is higher than the reactor volume, is also plotted as full lines. As expected the increase of β enlarges the efficiency of the reactor and for a given value of β the behaviour predicted for the rigorous model approaches that of Eq. (30) when R increases. The more pronounced difference between both equations is detected in the middle range of T. Likewise, the behaviour predicted by Eq. (30) is more efficient than that of the rigorous model, because the model according to Eq. (30) assumes that the electrochemical reactor is in steady state, which represents the maximal value of conversion per pass in the reactor.

Fig. 2 summarizes the behaviour of a stirred tank electrochemical reactor coupled with a reservoir according to Eqs. (28) and (30). The results are presented by using a contour plotting routine to produce iso-λ profiles, where

$$\lambda = \frac{C_{i,Eq.(28)}(T) - C_{i,Eq.(30)}(T)}{C_{i,Eq.(28)}(T)} \times 100 \tag{31}$$

T was evaluated according to Eq. (30) for a conversion factor of 0.5 in the reservoir. It is observed that the difference in the predictive behaviour between the two equations is significant at low values of β and R. Likewise, the λ values are always positive, which corroborates the more efficient performance predicted by Eq. (30) as observed in the previous figure.

2.1.5. Plug flow model (Pe → ∞), PF

When Pe → ∞, Eq. (8) becomes

$$\frac{1}{R}\frac{\partial C(T,y)}{\partial T} = -\frac{\partial C(T,y)}{\partial y} - \beta C(T,y) \tag{32}$$

Walker and Wragg [2] assumed as initial condition a steady state concentration distribution according to

$$T = 0 \quad C(0,y) = e^{-\beta y} \tag{33}$$

Thus, the rigorous solution of Eqs. (15) and (32) yields for the concentration in the reservoir:

$$C_i(T)|_{PF} = 1 + (1 - e^{\beta}) \int_0^T \sum_{n=0}^{\infty} \frac{(z - n/R)^n}{n!(e^{\beta})^{n+1}} e^{(-z+n/R)} dz \tag{34}$$

Schaller and Kreysa [4] suggested that a more realistic model is to consider a constant initial concentration in all the system. Thus, changing the initial condition Eq. (33) by Eq. (9), the concentration in the reservoir is given by

$$C_i(T)|_{PF} = e^{-\beta RT} \left[1 + \beta R e^{\beta} \int_0^T e^{\beta R z} \sum_{n=0}^{\infty} \frac{(z - n/R)^n}{n!(e^{\beta})^{n+1}} e^{(-z+n/R)} dz \right] \tag{35}$$

The derivation of Eq. (35) is given in Appendix A.

2.1.6. Plug flow model at high R values

At high Pe number Eq. (23) is simplified to

$$C_i(T)|_{PF,R\to\infty} = e^{-(1-e^{-\beta})T} \tag{36}$$

For small β values the exponential function can be expressed as

$$e^{\beta} \approx 1 + \beta \tag{37}$$

Introducing Eq. (37) into Eq. (36) gives Eq. (30) as a limiting case of Eq. (36).

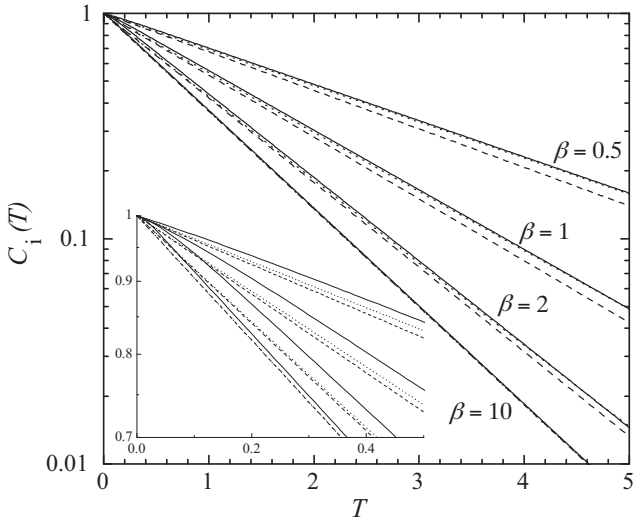

Fig. 3. Comparison of the concentration in the reservoir for a plug flow reactor coupled with a reservoir. Full line: Eq. (35); dotted line: Eq. (34); and dashed line: Eq. (36). $R = 10$. Inset: exploded view at low T values.

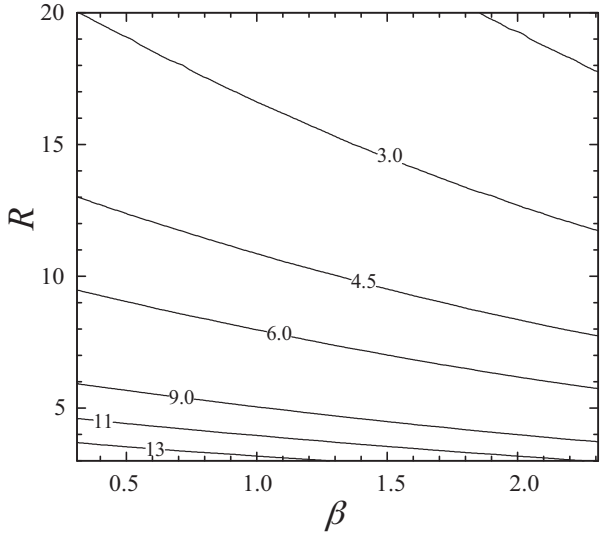

Fig. 5. Contour plots of λ, according to Eqs. (35) and (36), for a plug flow electrochemical reactor coupled with a reservoir as a function of R and β. Contour height numbers are λ values.

For $\beta \ll 1$ Eq. (30) is simplified to

$$C_i(T) = e^{-\beta T} \tag{38}$$

Taking into account Eq. (14) and assuming that the reservoir volume is approximately the total volume of electrolyte, Eq. (38) yields

$$C_i(t)|_{BR} = e^{-ka_e t} \tag{39}$$

valid for a batch reactor, BR.

Fig. 3 shows the temporal behaviour of an electrochemical reactor according to the plug flow model coupled with a reservoir. The behaviours predicted by the more accurate models, Eqs. (34) and (35), and the simplified model Eq. (36) are reported. It can be observed that both accurate models give similar performance and all the calculation procedures present the same performance when β is very high.

Fig. 4 shows the dimensionless concentration in reservoir as a function of dimensionless time at different values of β and R for an electrochemical plug flow reactor coupled with a reservoir, Eq. (35). The inset corresponds to the behaviour at the beginning of the experiment. The performance according to Eq. (36), assuming that the reservoir volume is higher than the reactor volume, is also plotted as full lines. Fig. 5 summarizes the iso-λ profiles for a plug flow electrochemical reactor coupled with a reservoir according to Eqs. (35) and (36). Figs. 4 and 5 show a similar performance to those of Figs. 1 and 2, which are valid for the stirred tank model.

Fig. 6 compares the concentration in the reservoir for recirculating electrochemical systems according to the axial dispersion model, numerical solution of Eq. (18), with those of the simplified treatments given by Eqs. (30) and (36). As expected Eq. (36) shows a reactor with the best performance and the temporal behaviour of the system is strongly dependent on the set of parameters β, R and Pe. To obtain the admissibility of application of the simplified models, Fig. 7 reports λ, used as a criterion of error estimation, for different values of the dimensionless parameters β, R and Pe.

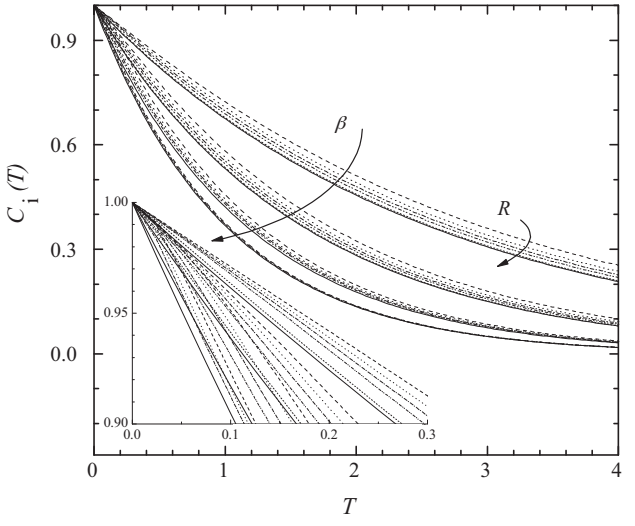

Fig. 4. Dimensionless reservoir concentration as a function of time for a plug flow electrochemical reactor coupled with a reservoir according to Eq. (35) for different values of β and R. β values: 0.5, 1, 2, and 10. R values: 5, 8, 12, 20, and 100. Full lines: behaviour according to Eq. (36). Inset: exploded view at low T values.

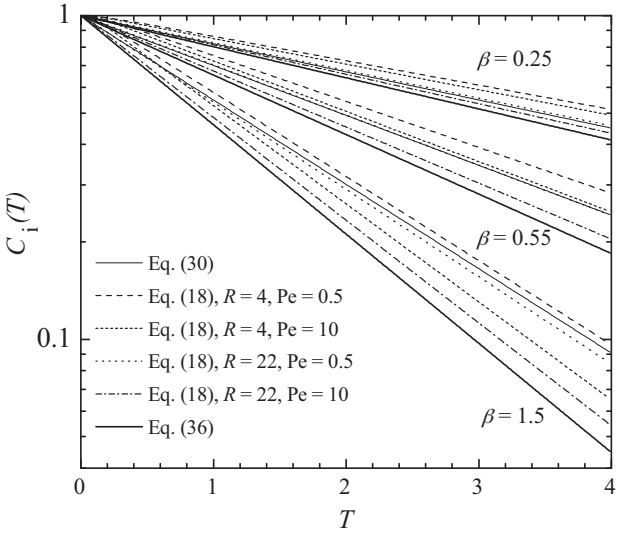

Fig. 6. Comparison of the dimensionless concentration in the reservoir as a function of time for the dispersion model, numerical solution of Eq. (18), with the simplified models given by Eqs. (30) and (36) for different values of β, R and Pe.

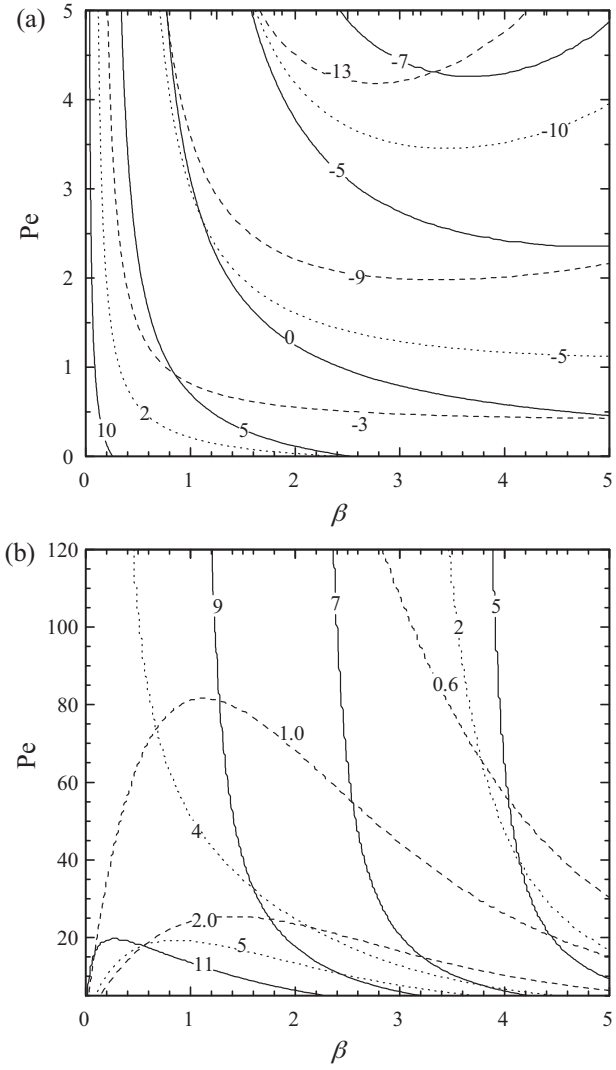

Fig. 7. Contour plots of λ. Part (a) λ was evaluated according to the numerical solution of Eq. (18) and Eq. (30). Part (b) λ was evaluated according to the numerical solution of Eq. (18) and Eq. (36). Full lines: $R = 5$; dotted lines: $R = 15$; and dashed lines: $R = 100$. Contour height numbers are λ values.

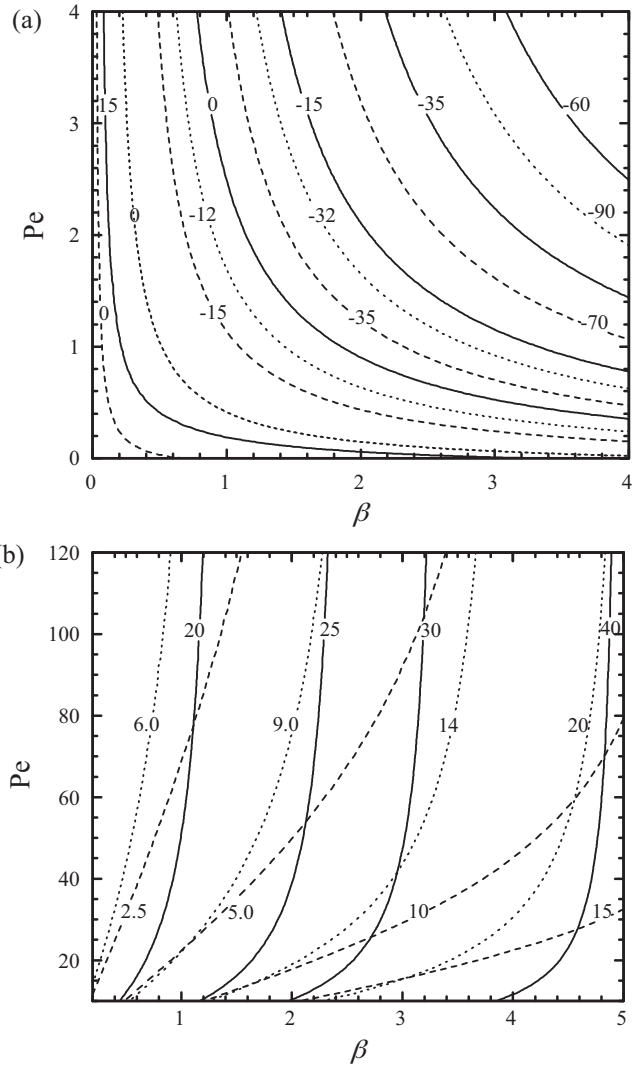

Fig. 8. Contour plots for the error in the evaluation of β. Part (a) Comparison between numerical solution of Eq. (18) with Eq. (30). Part (b) Comparison between numerical solution of Eq. (18) with Eq. (36). Full lines: $R = 5$; dotted lines: $R = 15$; and dashed lines: $R = 100$. Contour height numbers are error values.

Laboratory studies with recirculating electrochemical reactor systems are also frequently used to evaluate the kinetic constant. Thus, the error in the calculation of β defined as:

$$\text{Error} = \frac{\beta_{\text{Eq.(18)}} - \beta_{\text{Eq.(30) or Eq.(36)}}}{\beta_{\text{Eq.(18)}}} \times 100 \qquad (40)$$

is shown in Fig. 8 as iso-error profiles in terms of the Peclet number and β for different R values. The results of Eq. (18) are compared with those according to Eq. (30), valid for the stirred tank model at high R values, in Fig. 8(a) and with those of Eq. (36), plug flow model at high R values, in Fig. 8(b). It must be recognized that Eq. (18) takes into account two factors which are disregarded in Eqs. (30) and (36), i.e. (i) the temporal behaviour of the electrochemical reactor and (ii) the presence of dispersion. According to the first factor, the electrochemical reactor in Eqs. (30) and (36) is in steady state. Then, the correlation of experimental results with these equations requires β values lower than those of Eq. (18) and the error in the calculation of β must be positive for both simplified models. However, taking into account the presence of dispersion, the plug flow model is more efficient than the dispersion model, which requires that the β calculated with Eq. (36) must be lower than the value given by Eq. (18) and the error is also positive. In contrast, the behaviour of the stirred tank model is less efficient than the dispersion model and Eq. (30) yields β values higher than for Eq. (18), which produces negative errors. In conclusion, both factors show an opposite contribution when the dispersion model is compared with the stirred tank model. Thus, the error in the evaluation of β can be positive, negative or null depending on the predominance of each factor, as shown in Fig. 8(a). In this case it is possible that both factors have compensating effects and Eqs. (18) and (30) yield the same result for the evaluation of β. However, both factors contribute in the same direction when the dispersion model is compared with the plug flow model, which always gives positive errors, as shown in Fig. 8(b). Finally, Fig. 8 shows that the use of Eq. (30) or Eq. (36) for the correlation of experimental results instead of Eq. (18) can produce significant errors in the calculation of β depending on the fluid dynamics, mass-transfer behaviour and operating conditions of the recirculating electrochemical system.

According to Eqs. (18), (23), (30), (36) and (39) the logarithm of the concentration in the reservoir always shows a linear relationship with time. However, the true value of the kinetic constant, calculated from the slope of the line, depends on the mathematical model adopted to represent the electrochemical reactor. Thus, it is necessary to have additional information about the fluid dynamic

behaviour of the system in order to choose the appropriate equation to perform this calculation.

2.2. Current as a function of time at high R values

2.2.1. Dispersion model

In order to obtain the average current density, j_{mean} (A m^{-2}), as a function of time, Eq. (5) must be integrated

$$j_{mean}(T,y) = \nu_e F k c^0 \int_0^1 C(T,y)\mathrm{d}y \tag{41}$$

Introducing Eq. (20) into Eq. (41) and integrating gives

$$j_{mean}(T) = \frac{4\nu_e F k c^0 \left[\frac{\alpha+1}{\alpha-1}(e^{\alpha Pe/2} - e^{Pe/2}) + \frac{\alpha-1}{\alpha+1}(e^{Pe/2} - e^{-\alpha Pe/2})\right]}{Pe\left[(\alpha+1)^2 e^{\alpha Pe/2} - (\alpha-1)^2 e^{-\alpha Pe/2}\right]} \times C_i(T) \tag{42}$$

Introducing Eq. (23) into Eq. (42) and applying logarithms to both sides of this equation, yields

$$\ln j_{mean}(T)\big|_{DM,R\to\infty} = \ln\left\{\frac{4\nu_e F k c^0 \left[(\alpha+1)/(\alpha-1)(e^{\alpha Pe/2} - e^{Pe/2}) + (\alpha-1)/(\alpha+1)(e^{Pe/2} - e^{-\alpha Pe/2})\right]}{Pe\left[(\alpha+1)^2 e^{\alpha Pe/2} - (\alpha-1)^2 e^{-\alpha Pe/2}\right]}\right\} - \left[1 - \frac{4\alpha e^{Pe/2}}{(\alpha+1)^2 e^{\alpha Pe/2} - (\alpha-1)^2 e^{-\alpha Pe/2}}\right] T \tag{43}$$

2.2.2. Plug flow model

Solving Eq. (32) at high R values, introducing the result into Eq. (41) and integrating, yields

$$j_{mean}(T) = \frac{\nu_e F k c^0}{\beta}(1 - e^{-\beta}) C_i(T) \tag{44}$$

Introducing Eq. (36) into Eq. (44) and applying logarithms to both sides of the resulting equation, yields

$$\ln j_{mean}(T)\big|_{PF,R\to\infty} = \ln\left[\frac{\nu_e F k c^0}{\beta}(1 - e^{-\beta})\right] - (1 - e^{-\beta})T \tag{45}$$

2.2.3. Stirred tank model

Solving Eq. (24) at high R values, introducing the result into Eq. (41) and combining with Eq. (30), results in

$$\ln j_{mean}(T)\big|_{ST,R\to\infty} = \ln\left(\frac{\nu_e F k c^0}{1+\beta}\right) - \left(\frac{\beta}{1+\beta}\right) T \tag{46}$$

Eq. (46) was firstly reported by Robinson and Walsh [13]. In all cases it is observed that the dependence of current with time in semi-log coordinates is always a straight line, whose slope and ordinate depend on the model used to represent the electrochemical system. Likewise, for a given model in semi-log coordinates, the temporal variation of current shows the same slope as that for the change in concentration. However, for the evaluation of β it is more appropriate to use the concentration variation because the current can be influenced by side reactions, which occur at the electrode simultaneously with the main reaction.

3. Residence time distribution

For an electrochemical system without reaction Eq. (1) is simplified to:

$$\frac{\partial c(t,y)}{\partial(t/t_{mean})} = \frac{1}{Pe}\frac{\partial^2 c(t,y)}{\partial y^2} - \frac{\partial c(t,y)}{\partial y} \tag{47}$$

Considering an impulse function as a stimulus the initial and boundary conditions for a closed system are given by

$$t = 0 \quad c(0,y) = a\delta(y-0) \tag{48}$$

$$y = 0 \quad \text{and} \quad t > 0^+ \quad c(t,0) - \frac{1}{Pe}\left.\frac{\partial c(t,y)}{\partial y}\right|_{y=0} = 0 \tag{49}$$

$$y = 1 \quad \left.\frac{\partial c(t,y)}{\partial y}\right|_{y=1} = 0 \tag{50}$$

here a is a parameter and δ is the Dirac delta function.

The normalized outlet concentration, termed the E curve [14], was calculated as

$$E(t) = \frac{c(t,1)}{\int_0^\infty c(t,1)\mathrm{d}(t/t_{mean})} \tag{51}$$

In these studies a dimensionless time referred to the mean residence time, t_{mean} (s), was used, which was calculated as

$$t_{mean} = \frac{\int_0^\infty tc(t)\mathrm{d}t}{\int_0^\infty c(t)\mathrm{d}t} \tag{52}$$

The experimental data were correlated by means of the least squares method applied to Eq. (47) and using the Peclet number as fitting parameter. Eq. (47) was numerically solved by the tridiagonal matrix algorithm (TDMA) [15]. To quantify the agreement between theoretical and experimental data, the mean square error, MSE, is introduced as

$$MSE = \frac{1}{N-1}\sum_{i=1}^{N}(E_i^{th} - E_i^{exp})^2 \tag{53}$$

The Peclet number for which MSE is minimal is then taken as the best fit value [16].

4. Experimental

Fig. 9(a) shows the configuration of the undivided continuous electrochemical reactor used in this work, 109 mm internal diameter and 201 mm total high, with a rotating cylinder electrode. The upper end of the cylinder was attached to the motor shaft. A helical platinum wire (1.0 mm diameter × 1 m long) with an internal diameter of 55 mm was used as counterelectrode. The working electrode and the counterelectrode were concentric, thereby ensuring a uniform primary current distribution. The reactor was made in acrylic and was included in a flow circuit system, shown in Fig. 9(c) including a centrifugal pump, a flowmeter, a diaphragm valve a reservoir and a thermostat.

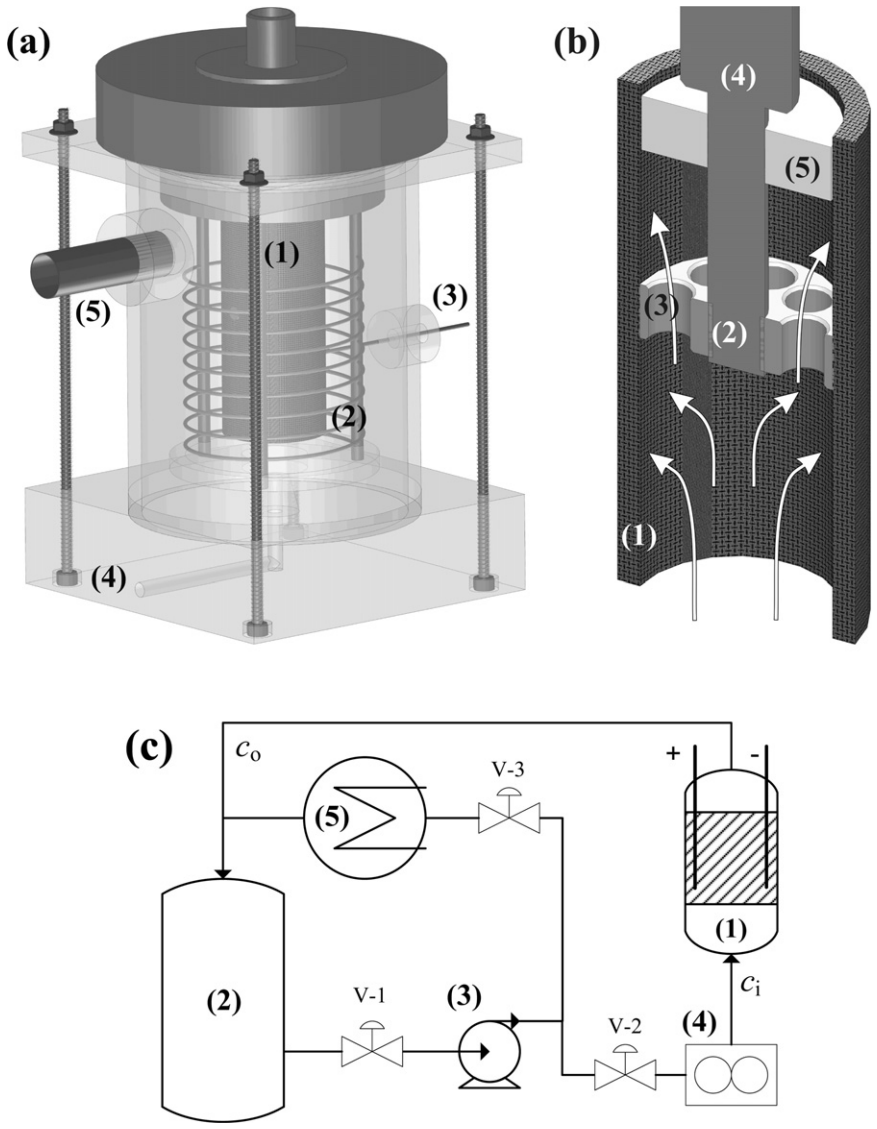

Fig. 9. (a) Schematic representation of the reactor. (1) Rotating cylinder cathode; (2) helical anode; (3) Luggin probe to reference electrode; (4) reactor inlet; and (5) reactor outlet. (b) Exploded view of the hollow three-dimensional rotating cylinder electrode. (1) Three-dimensional electrode; (2) electrical contact; (3) perforated brass disc; (4) electrode shaft; and (5) Teflon disc. *Arrows*: electrolyte flow. (c) Scheme of the electrolyte circulation system. (1) Reactor; (2) reservoir; (3) pump; (4) flow meter; and (5) thermostat; (V-1, V-2 and V-3) valves.

For the evaluation of the performance of the recirculating electrochemical system two types of rotating cylinder electrodes were used. The first was a smooth stainless steel cylinder (32 mm diameter × 90 mm long, 90.5 cm^2 electrode surface area), and the second one was made by winding a 304 stainless steel wire mesh (25-mesh size, 0.30 mm wire diameter and 0.72 mm distance between wires) around a detachable cylinder, 35 mm diameter, which was removed afterwards the external layer was welded at several points to obtain mechanical stability of the structure. Thus a hollow three dimensional electrode was obtained as shown in Fig. 9(b), with 43 mm outer diameter and 90 mm long. The average value of the geometric specific surface area was approximately 3724 m^{-1} with a void fraction of 0.7. The three dimensional electrode was supported by two discs. One of them, centrally positioned, was a perforated brass disc and a stainless steel bolt passed through the bed thickness, pressing the central disc and thus ensuring electrical contact. The lower part of the electrode was open but the upper part was joined to a Teflon disc in order to orientate the electrolyte flow through the sheet pack. The central disc and the electrode shaft were covered with epoxy resin to make them electrochemically inactive. Copper deposition from dilute solutions and oxygen evolution were used as cathodic and anodic reactions, respectively. The solution was prepared by dissolving copper sulphate in 1 M sodium sulphate solution, pH 2 with the addition of H_2SO_4, to achieve an initial copper concentration of approximately 500 mg dm^{-3}, when the smooth electrode was used; and lower than 200 mg dm^{-3} for the case of the three-dimensional electrode. In the experiments with smooth electrodes the solution volume in the reactor was 1 dm^3 and 5 dm^3 in the reservoir, whereas for a recirculating system with the three-dimensional electrode the solution volumes in the reactor and reservoir were 0.87 dm^3 and 10.13 dm^3, respectively. These experiments were performed under potentiostatic control, maintaining the cathode potential at −0.55 V against a saturated calomel electrode as reference. During the experiments, small volumes of solution were taken out from the reservoir at different times and the copper concentration was determined by atomic absorption spectroscopy to obtain the concentration versus time curve, and the current was monitored with a digital multimeter. All experiments were performed at 30 °C.

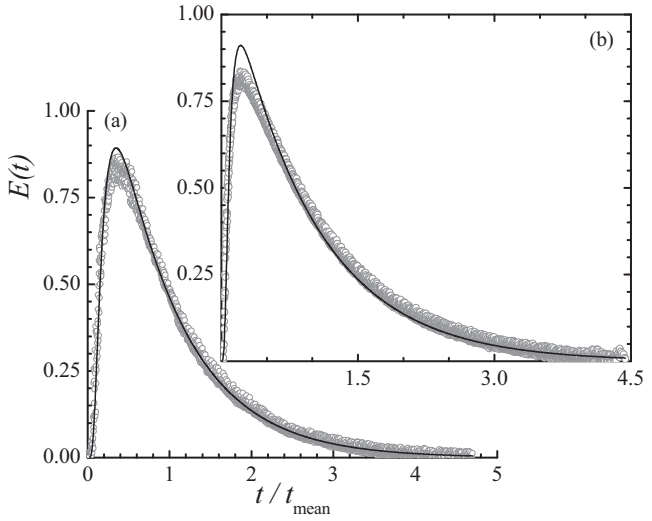

Fig. 10. Residence time distribution. (a) Smooth rotating cylinder electrode, $Q = 3.78 \times 10^{-5}\ m^3\ s^{-1}$, $\omega = 146.6\ s^{-1}$, Pe = 1.32. (b) Hollow three-dimensional rotating cylinder electrode, $Q = 3.25 \times 10^{-6}\ m^3\ s^{-1}$, $\omega = 62.8\ s^{-1}$, Pe = 0.58. Full lines: Correlation according to Eq. (47), numerically solved.

The residence time distribution was analyzed for smooth rotating cylinders, 90 mm long, with the following diameters: 20, 32 and 42 mm and also for the hollow three-dimensional rotating cylinder electrode above described. As a stimulus, an instantaneous tracer injection of 0.2 cm^3 of a 30 wt% NaOH solution was manually introduced at the reactor inlet. The electrolytic conductivity was monitored by means of a platinum conductivity cell, WTW model LTA 01, with a cell constant 0.114 cm^{-1} mounted on a T-piece in the reactor outlet. The conductimeter was connected to a digital multimeter to obtain conductance versus time.

5. Results and discussion

5.1. Residence time distribution results

Fig. 10 shows typical curves of the normalized outlet concentration at a given flow rate, $Q\ (m^3\ s^{-1})$, and rotation speed, $\omega\ (s^{-1})$, for the smooth and for the hollow three-dimensional cylinder electrodes. The experimental points correspond to three independent experiments and the full lines represent the numerical fitting of the experimental results with Eq. (47), where a close correlation is observed. The correlated value of the Peclet number for the smooth electrode was 1.32 and 0.58 for the three-dimensional case. Coeuret and Storck [17] and Eklund and Simonsson [18] reported a successfully correlation of experimental mass-transfer coefficients for a rotating cylinder electrode with axial flow taking as characteristic length the difference between the reactor radius and the electrode radius. They used an axial Reynolds number, Re_a, and a Taylor number, Ta, to consider the axial and rotational flows, respectively, which are defined as:

$$Re_a = \frac{4Q(D-d)}{\pi(D^2-d^2)\nu} \tag{54}$$

and

$$Ta = \frac{d\omega(D-d)}{4\nu} \times \left(\frac{D-d}{d}\right)^{0.5} \tag{55}$$

where $d\ (m)$ is the electrode diameter, $D\ (m)$ is the reactor diameter and $\nu\ (m^2\ s^{-1})$ is the kinematic viscosity.

Thus, the Bodenstein number, Bo, is given by

$$Bo = \frac{Pe(D-d)}{L} \tag{56}$$

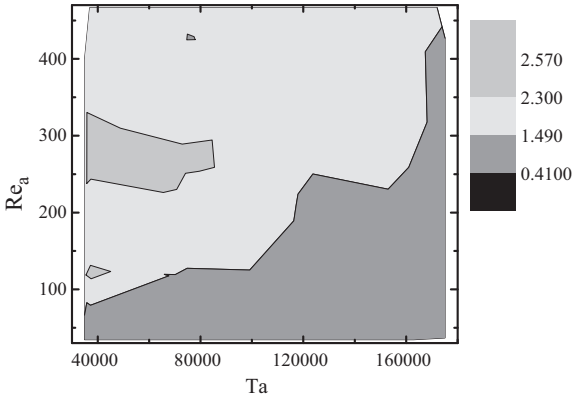

Fig. 11. Contour plots of Bodenstein number for smooth rotating cylinder electrodes as a function of axial Reynolds and Taylor numbers. Contour height numbers are Bo values.

Fig. 11 shows a contour plot of iso-Bodenstein number profiles as a function of both the axial Reynolds number and the Taylor number for smooth rotating cylinders. The measurements were carried out at $31.4 < \omega < 146.6\ s^{-1}$ and $0.325 < Q < 3.78 \times 10^{-5}\ m^3\ s^{-1}$. Within the accuracy normally expected for this type of measurements, three regions can be observed. A first zone is detected at low values of Re_a or at high Ta, where Bo ranges from 0.4 to 1.5. This zone is under well mixed conditions and is characterized for the lower values of Bo. The second region is identified for Bo ranging from 1.5 to 2.3, where the influence of the axial flow is more important. The third zone, detected as an island with the highest Bo, occurs in the middle range of Re_a at low Ta. However, it is necessary to emphasize that the Bodenstein number shows a variation in a narrow range, from 0.4 to 2.6, in spite of the broad experimental conditions.

Fig. 12 shows the Peclet number as a function of the Taylor number for a hollow three-dimensional rotating cylinder at different axial Reynolds numbers. The measurements were carried out at $20.9 < \omega < 62.8\ s^{-1}$ and $0.325 < Q < 3.78 \times 10^{-5}\ m^3\ s^{-1}$. The secondary ordinate axis on the right hand side of the graph corresponds to the Bodenstein number. As expected the Peclet number decreases with increase in rotation speed because of the improvement in the mixing conditions and the flow rate has a small influence. Likewise, the hollow three-dimensional electrode shows Bodenstein numbers lower than the smooth rotating electrodes, which can be attributed to the flow of the electrolyte through the sheet pack.

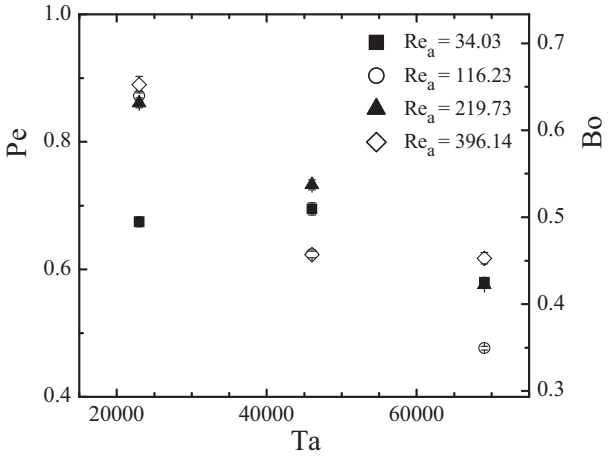

Fig. 12. Peclet and Bodenstein numbers as a function of the Taylor number for a hollow three-dimensional rotating electrode.

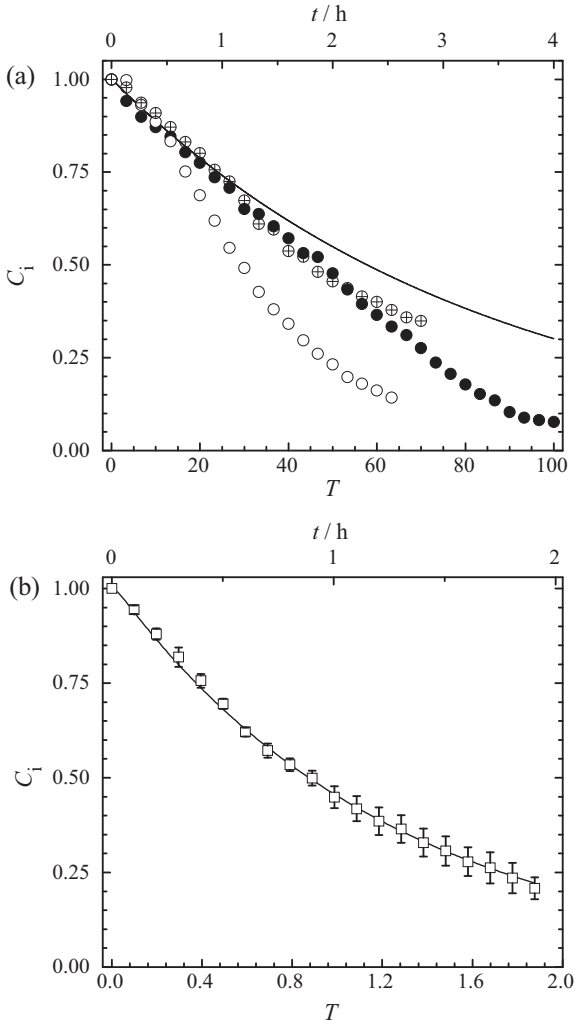

Fig. 13. Concentration in the reservoir as a function of time. Cathode potential versus SCE: −0.55 V. (a) Smooth rotating electrode. The circles represent three independent experiments. c (0) = 537 ± 19 mg dm^{-3}, $Q = 3.47 \times 10^{-5}$ m^3 s^{-1}, $\omega = 146.6$ s^{-1}, Pe = 1.32, $R = 5$. (b) Hollow three-dimensional rotating electrode. (□) mean value of three independent experiments, the segments represent the standard deviation. c (0) = 174 ± 30 mg dm^{-3}, $Q = 2.77 \times 10^{-6}$ m^3 s^{-1}, $\omega = 62.8$ s^{-1}, Pe = 0.58, $R = 11.64$. Full line: numerical solution of Eq. (18).

5.2. Temporal behaviour of concentration in the reservoir

Fig. 13 shows typical results of the concentration in the reservoir as a function of time for two rotating cylinder electrodes. Fig. 13(a) shows the results for the smooth cylinder electrode for three independent experiments and those of the three-dimensional rotating electrode are given in Fig. 13(b). In this last case each point represents the mean value of three independent experiments and the segments the standard deviation. Both electrodes show a similar behaviour. For time values lower than 45 min a close agreement is observed between independent experiments, and the results show scatter at time higher than 1 h because of the unpredictable increase in the specific surface area due to metal deposition. This behaviour is more pronounced for the smooth rotating cylinder electrode due to the higher copper concentration and to the longer duration of the experiments to achieve a similar value of dimensionless concentration in the reservoir. The experimental results were correlated by means of the least squares method applied to Eq. (18), numerically solved and plotted in Fig. 13, using β as fitting parameter. The same procedure was performed with Eqs. (23), (28) and (30). The last equation, in linearized form, is the conventional relationship used to fit experimental results in recirculating electrochemical systems in order to obtain the kinetic constant. In these calculations the Peclet number was taken from Fig. 10. For the smooth electrode only the points at T values lower than 30 were used in the correlation due to scatter at high times. Table 1 summarizes the correlation data, β and the mean square error for each equation are reported. The last four columns in Table 1 show the error in the calculation of β for the different equations, related to the value given by the rigorous model, Eq. (18). For a given electrode kind, it can be observed that the mean square error is similar for all the equations. Thus they present a comparable correlation capability of the experimental results but with a different β value. For the smooth rotating electrode, under the examined experimental conditions, Eq. (30) gives an error of 8.3% in comparison with the value of Eq. (18). This error is in accordance with the values reported on Fig. 8(a), where it can be seen that for low values of β the error between the behaviour of Eqs. (18) and (30) is independent of Pe number. On the other hand, Eq. (18) gives same result as Eq. (28) and Eq. (23) agrees with Eq. (30), both in the normal and in the linearized form. Thus, in this case the temporal behaviour of the electrochemical reactor has a strong influence on the recirculating system and the effect of the dispersion can be neglected. The last row in Table 1 summarizes the correlation capability for the Eqs. (18), (23), (28) and (30) for the hollow three-dimensional rotating electrode. All the equations show significant errors in comparison with the β value given by Eq. (18). It must be emphasized that Eq. (30) in the linearized form, which represents the ordinary procedure for the processing of data, gives an error of −26.3. This value also agrees with the prediction of Fig. 8(a). It must be recognized that the errors reported here are higher than the value reported by Mustoe and Wragg [3]. Thus, depending on its geometric, fluid dynamic and physicochemical properties is necessary to take into account a more complex model to represent a recirculating electrochemical system.

6. Engineering aspects of the mathematical models

An electrochemical reactor with a rotating cylinder electrode is frequently assumed as a well mixed system. According to the previous sections the use of a simplified model allows an easy method to calculate the kinetic constant but it is possibly subject to high error. In contrast the dispersion model gives more exact values but requires the use of complicated mathematical calculations. In order to circumvent these difficulties, the aim of this section is to show graphically the error in the evaluation of the kinetic constant according to the dispersion model at high R values, Eq. (23), when this equation is used instead of the rigorous treatment given by the dispersion model, Eq. (18) solved by a numerical procedure. Thus, Fig. 14 shows the β value according to Eq. (23) as a function of m, given by

$$m = \left.\frac{d \ln C_i(T)}{dT}\right|_{exp} \tag{57}$$

and for different Peclet numbers. The inset in Fig. 14 reports θ, defined as

$$\theta = \frac{\beta_{DM}}{\beta_{DM,R\to\infty}} \tag{58}$$

as a function of m for different R values and Peclet numbers. Therefore, the use of Fig. 14 to evaluate β requires the calculation of m by correlation of experimental results. Introducing m as abscissae and choosing a Peclet number it can obtain β for the dispersion model at high R values. Introducing m and choosing the R and Pe values the inset in Fig. 14 yields θ as ordinate, which allows the calculation of β according to the dispersion model. It can be observed that significant errors in the evaluation of β can be obtained for low values of R.

Table 1
Summary of correlation data.

Electrode kind	$Q \times 10^6$ ($m^3\ s^{-1}$)	Eq. (18)		Eq. (23)		Eq. (28)		Eq. (30)		Eq. (30) linear		Error (%)			
		β	MSE	β	MSE	β	MSE	β	MSE	β	MSE	Eq. (23)	Eq. (28)	Eq. (30)	Eq. (30) linear
Smooth electrode $\beta \times 10^2$, MSE $\times 10^3$	34.72	1.32	0.31	1.21	0.31	1.32	0.31	1.21	0.31	1.21	0.29	8.3	0	8.3	8.3
Three-dimensional $\beta \times 10^0$, MSE $\times 10^3$	2.77	3.35	0.62	3.01	0.71	4.25	0.63	3.84	0.71	4.23	0.73	10.1	−26.9	−14.6	−26.3

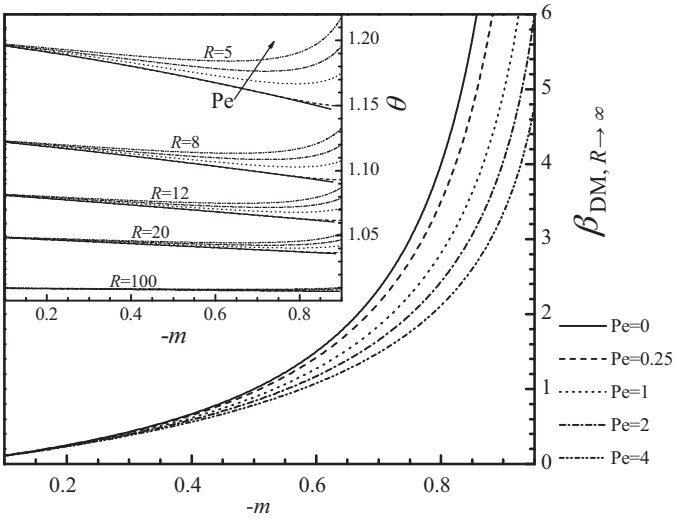

Fig. 14. β according to Eq. (23) as a function of the experimental slope value, m, for different Peclet numbers. Inset: Ratio between β according to the rigorous dispersion model to β according to Eq. (23) as a function of m for different R values and Peclet numbers.

7. Conclusions

(a) When the reactor can be represented by the stirred tank model, the temporal behaviour of a recirculating system can be modelled assuming the reactor in steady state only when β is higher than 1 and the ratio between the reservoir space time to the reactor space time, R, is higher than 15. In this case the error in the predictions is lower than 3%. However, the exact value of the error depends on β and R.

(b) When the reactor can be represented by the plug flow model, the temporal behaviour of a recirculating system can be modelled assuming the reactor in steady state only when β is higher than 1.5 and R is higher than 15. In this case the error in the predictions is lower than 3%. However, the exact value of the error depends on β and R.

(c) The hydrodynamic behaviour of a rotating cylinder can be properly represented by the dispersion model. The Peclet number lay in the range 0.4–3.2 for the smooth or three-dimensional electrodes examined in this work. The exact value of the Peclet number depends on both the Reynolds and Taylor numbers.

(d) Using a recirculating electrochemical reactor system it is very important to verify the hydrodynamic behaviour of the reactor and to take into account the ratio between the reactor volume to the reservoir volume in order to adopt the most appropriate model for the calculation of the kinetic constant from experimental results. Despite the fact that all the models predict that the logarithm of the concentration in the reservoir shows a linear relationship with time, the use of the incorrect equation can produce a high error in the evaluation of the kinetic constant. Thus, from the correlation of experimental data for the removal of copper with a hollow three-dimensional rotating cylinder electrode, it was demonstrated that the error in the evaluation of the kinetic constant can be as high as 26%.

Acknowledgements

This work was supported by the Agencia Nacional de Promoción Científica y Tecnológica (ANPCyT), Consejo Nacional de Investigaciones Científicas y Técnicas (CONICET) and Universidad Nacional del Litoral (UNL) of Argentina.

Appendix A. Deduction of Eq. (35)

Applying Laplace transformation to Eq. (32), integrating and evaluating at $y = 1$, yields

$$\bar{C}_o(s) = \frac{1}{(s+\beta R)}\left(1 - \frac{e^{-s/R}}{e^{\beta}}\right) + \bar{C}_i(s)\frac{e^{-s/R}}{e^{\beta}} \tag{A.1}$$

Applying Laplace transformation to Eq. (15) and combining to Eq. (A.1), is

$$\bar{C}_i(s) = \frac{1}{(s+\beta R)}\left[1 + \frac{\beta R e^{\beta}}{(s+1)e^{\beta} - e^{-s/R}}\right] \tag{A.2}$$

Thus, the inverse Laplace transformation of the first term on the right hand side is

$$\Im^{-1}\left[\frac{1}{(s+\beta R)}\right] = e^{-\beta RT} \tag{A.3}$$

To obtain the inverse Laplace transformation of the second term on the right hand side in Eq. (A.2) it must be noted that

$$\frac{1}{(s+1)e^{\beta} - e^{-s/R}} = \frac{1}{(s+1)e^{\beta}}\left[1 - \frac{e^{-s/R}}{(s+1)e^{\beta}}\right]^{-1} \tag{A.4}$$

Eq. (A.4) may be written as a power series expansion as

$$\frac{1}{(s+1)e^{\beta}}\left[1 - \frac{e^{-s/R}}{(s+1)e^{\beta}}\right]^{-1} = \sum_{n=0}^{\infty}\frac{e^{-ns/R}}{\left[(s+1)e^{\beta}\right]^{n+1}} \tag{A.5}$$

Multiplying top and bottom of the right hand side in Eq. (A.5) by $n!$ and taking into account the following definite integral

$$\frac{n!}{a^{n+1}} = \int_0^{\infty} x^n e^{-ax} dx \tag{A.6}$$

yields

$$\frac{1}{(s+1)e^{\beta} - e^{-s/R}} = \int_0^{\infty} e^{-x}\sum_{n=0}^{\infty}\frac{x^n e^{-(x+n/R)s}}{n!(e^{\beta})^{n+1}} dx \tag{A.7}$$

Defining

$$x = z - \frac{n}{R} \tag{A.8}$$

is

$$\frac{1}{(s+1)e^{\beta} - e^{-s/R}} = \int_0^{\infty} e^{-sz}\sum_{n=0}^{\infty}\frac{(z-n/R)^n e^{(-z+n/R)}}{n!(e^{\beta})^{n+1}} dz \tag{A.9}$$

Taking the inverse Laplace transformation of Eq. (A.9) results in

$$\Im^{-1}\left[\frac{1}{(s+1)e^{\beta} - e^{-s/R}}\right] = \sum_{n=0}^{\infty}\frac{(z-n/R)^n}{n!(e^{\beta})^{n+1}} e^{(-z+n/R)} \tag{A.10}$$

Applying the Borel theorem of convolution to the second term of the right hand side of Eq. (A.2) and taking into account Eq. (A.10) yields

$$\Im^{-1}\left[\frac{\beta R e^{\beta}}{(s+\beta R)[(s+1)e^{\beta} - e^{-s/R}]}\right]$$

$$= \beta R e^{\beta} e^{-\beta RT}\int_0^T e^{\beta Rz}\sum_{n=0}^{\infty}\frac{(z-n/R)^n}{n!(e^{\beta})^{n+1}} e^{(-z+n/R)} dz \tag{A.11}$$

Combining Eqs. (A.3) and (A.11) results in

$$C_i(T) = e^{-\beta RT}\left[1 + \beta R e^{\beta}\int_0^T e^{\beta Rz}\sum_{n=0}^{\infty}\frac{(z-n/R)^n}{n!(e^{\beta})^{n+1}} e^{(-z+n/R)} dz\right] \tag{A.12}$$

References

[1] D.J. Pickett, Electrochim. Acta 18 (1973) 835.
[2] A.T.S. Walker, A.A. Wragg, Electrochim. Acta 22 (1977) 1129.
[3] L.H. Mustoe, A.A. Wragg, J. Appl. Electrochem. 8 (1978) 467.
[4] C. Schaller, G. Kreysa, Chem.-Ing.-Tech. 58 (1986) 446.
[5] G.F. Thomas, K. Sora, Electrochim. Acta 32 (1987) 673.
[6] F. Rodriguez-Valadez, C. Ortiz-Éxiga, J.G. Ibanez, A. Alatorre-Ordaz, S. Gutierrez-Granados, Environ. Sci. Technol. 39 (2005) 1875.
[7] J.L. Nava, E. Sosa, G. Carreño, C. Ponce de León, M.T. Oropeza, Electrochim. Acta 51 (2006) 4210.
[8] M.R.V. Lanza, R. Bertazzoli, Ind. Eng. Chem. Res. 41 (2002) 22.
[9] K. Scott, Electrochemical Reaction Engineering, Academic Press, London, 1991, p. 54 (Chapter 2).
[10] R.G. Rice, D.D. Duong, Applied Mathematics and Modeling for Chemical Engineers, John Wiley & Sons, New York, 1995, p. 383 (Chapter 9).
[11] K.J. Hollenbeck, INVLAP.M: A matlab function for numerical inversion of Laplace transforms by the de Hoog algorithm, http://www.isva.dtu.dk/staff/karl/invlap.htm, 1998.
[12] T.Z. Fahidy, Principles of Electrochemical Reactor Analysis, Elsevier, Amsterdam, 1985, p. 137 (Chapter 6).
[13] D. Robinson, F.C. Walsh, Hydrometallurgy 26 (1991) 115.
[14] P.V. Danckwerts, Chem. Eng. Sci. 2 (1953) 1.
[15] S.D. Conte, C.W. de Boor, Elementary Numerical Analysis: An Algorithmic Approach, 3rd ed., McGraw-Hill, New Auckland, 1980, p. 153 (Chapter 4.2).
[16] A.N. Colli, J.M. Bisang, Electrochim. Acta 56 (2011) 7312.
[17] F. Coeuret, A. Storck, Elements de Genie Electrochimique, TEC&DOC, Paris, 1984, p. 138 (Chapter 3b).
[18] A. Eklund, D. Simonsson, J. Appl. Electrochem. 18 (1988) 710.